Journal of Biomechanics 43 (2010) 2281–2287

Contents lists available at ScienceDirect

Journal of Biomechanics

journal homepage: www.elsevier.com/locate/jbiomech
www.JBiomech.com

# Computational fluid dynamics analysis of cyclist aerodynamics: Performance of different turbulence-modelling and boundary-layer modelling approaches

Thijs Defraeye [a,*], Bert Blocken [b], Erwin Koninckx [c], Peter Hespel [c], Jan Carmeliet [d,e]

[a] Laboratory of Building Physics, Department of Civil Engineering, Katholieke Universiteit Leuven, Kasteelpark Arenberg 40, 3001 Heverlee, Belgium
[b] Building Physics and Systems, Eindhoven University of Technology, P.O. Box 513, 5600 Eindhoven, The Netherlands
[c] Research Centre for Exercise and Health, Department of Biomedical Kinesiology, Katholieke Universiteit Leuven, Tervuursevest 101, 3001 Heverlee, Belgium
[d] Chair of Building Physics, Swiss Federal Institute of Technology Zurich (ETHZ), Wolfgang-Pauli-Strasse 15, 8093 Zürich, Switzerland
[e] Laboratory for Building Science and Technology, Swiss Federal Laboratories for Materials Testing and Research (Empa), Überlandstrasse 129, 8600 Dübendorf, Switzerland

ARTICLE INFO

*Article history:*
Accepted 29 April 2010

*Keywords:*
Computational fluid dynamics
Turbulence model
Cyclist
Aerodynamics
Wind tunnel

ABSTRACT

This study aims at assessing the accuracy of computational fluid dynamics (CFD) for applications in sports aerodynamics, for example for drag predictions of swimmers, cyclists or skiers, by evaluating the applied numerical modelling techniques by means of detailed validation experiments. In this study, a wind-tunnel experiment on a scale model of a cyclist (scale 1:2) is presented. Apart from three-component forces and moments, also high-resolution surface pressure measurements on the scale model's surface, i.e. at 115 locations, are performed to provide detailed information on the flow field. These data are used to compare the performance of different turbulence-modelling techniques, such as steady Reynolds-averaged Navier–Stokes (RANS), with several $k$–$\varepsilon$ and $k$–$\omega$ turbulence models, and unsteady large-eddy simulation (LES), and also boundary-layer modelling techniques, namely wall functions and low-Reynolds number modelling (LRNM). The commercial CFD code Fluent 6.3 is used for the simulations. The RANS shear-stress transport (SST) $k$–$\omega$ model shows the best overall performance, followed by the more computationally expensive LES. Furthermore, LRNM is clearly preferred over wall functions to model the boundary layer. This study showed that there are more accurate alternatives for evaluating flow around bluff bodies with CFD than the standard $k$–$\varepsilon$ model combined with wall functions, which is often used in CFD studies in sports.



## 1. Introduction

At racing speeds ($\pm 50$ km/h in time trails), the aerodynamic resistance experienced by a cyclist, also called drag, is about 90% of his total resistance (Grappe et al., 1997; Kyle and Burke, 1984). The major part is caused by form drag, related to the position of the cyclist on the bicycle. Many elite cyclists therefore try to optimise their position for drag by means of field tests or wind-tunnel tests. With these techniques, the aerodynamic improvements are usually assessed by trial and error, by evaluating the drag reduction. Rarely these improvements are analysed more in detail by considering the resulting changes in the flow field since measurements of the flow field are often time-consuming and can even be quite difficult to set up for field tests. An alternative technique, which provides both drag and detailed flow-field information, is computational fluid dynamics (CFD), which has recently been used in cycling (Defraeye et al., 2010; Hanna, 2002; Lukes et al., 2004) but also in other sports disciplines like swimming (Bixler et al., 2007; Bixler and Riewald, 2002; Bixler and Schloder, 1996; Gardano and Dabnichki, 2006; Lecrivain et al., 2008; Minetti et al., 2009; Rouboa et al., 2006; Zaïdi et al., 2008; Zaïdi et al., 2010), soccer (Barber et al., 2009), bobsleighing (Dabnichki and Avital, 2006) and ski jumping (Meile et al., 2006). All these studies consider flow around bluff bodies, i.e. mostly humans, which have a quite streamlined shape (i.e. without sharp edges) and therefore no fixed boundary-layer separation points, in contrast to other (sharp-edged) bluff bodies such as buildings. For these types of flows, the CFD modelling approaches, applied in the aforementioned studies (see Table 1), have some limitations: (1) using steady Reynolds-averaged Navier–Stokes (RANS) modelling, the unsteady motions in the wake of a bluff body are not captured. Only the mean flow is resolved and all scales of turbulence are modelled by a turbulence model. There is however no universally valid turbulence model which is accurate for all classes of flows (Casey and Wintergerste, 2000); (2) using wall functions, the flow quantities in the boundary layer at the wall are modelled instead of being resolved. Since wall functions are only valid under strict conditions, they can result in inaccurate

* Corresponding author. Tel.: +32 16321348; fax: +32 16321980.
*E-mail address:* thijs.defraeye@bwk.kuleuven.be (T. Defraeye).

0021-9290/$ - see front matter © 2010 Elsevier Ltd. All rights reserved.
doi:10.1016/j.jbiomech.2010.04.038

**Table 1**
Overview of turbulence and boundary-layer modelling approaches of previous CFD studies in sports.

| Author | Application | 2D/3D | Steady/unsteady | Turbulence and BL modelling | Validation |
|---|---|---|---|---|---|
| Bixler and Schloder (1996) | Swimming (hand) | 2D | Steady/unsteady[b] | s$k$–$\varepsilon$, rng$k$–$\varepsilon$, RSM | Drag force[a] |
| Bixler and Riewald (2002) | Swimming (arm) | 3D | Steady | s$k$–$\varepsilon$ (NWF) | Drag and lift force[a] |
| Dabnichki and Avital (2006) | Bobsleighing (bob and riders) | 3D | Steady | s$k$–$\omega$ (WF) | Drag and lift force+FV |
| Gardano and Dabnichki (2006) | Swimming (arm) | 3D | Steady | – | Drag and lift force |
| Meile et al. (2006) | Ski jumping (skier) | 3D | Steady | s$k$–$\varepsilon$ | Drag and lift force |
| Rouboa et al. (2006) | Swimming (arm) | 2D | Steady/unsteady[b] | s$k$–$\varepsilon$ | Drag and lift force[a] |
| Bixler et al. (2007) | Swimming (swimmer) | 3D | Steady | s$k$–$\varepsilon$ (NWF) | Drag force |
| Barber et al (2009) | Soccer (balls) | 3D | Steady | r$k$–$\varepsilon$ (LRNM) | Drag force+FV |
| Lecrivain et al. (2008) | Swimming (swimmer) | 3D | Unsteady[c] | – | Drag force [a] |
| Zaïdi et al. (2008) | Swimming (swimmer) | 2D | Steady | s$k$–$\varepsilon$ (NWF) | – |
| Zaïdi et al. (2010) | Swimming (swimmer) | 3D | Steady | s$k$–$\varepsilon$ (NWF), s$k$–$\omega$ (WF) | Drag force[a]+FV |
| Defraeye et al. (2010) | Cycling (cyclist) | 3D | Steady/unsteady[d] | s$k$–$\varepsilon$ (LRNM), LES (LRNM) | Drag force and surface pressures |

s$k$–$\varepsilon$: standard $k$–$\varepsilon$ model; s$k$–$\omega$: standard $k$–$\omega$ model; rng$k$–$\varepsilon$: RNG $k$–$\varepsilon$ model; RSM: Reynolds stress model; r$k$–$\varepsilon$: realizable $k$–$\varepsilon$ model; WF: wall functions; NWF: non-equilibrium wall functions; FV: flow visualisation; BL: boundary-layer.

[a] Validation was performed by comparison with data of previous experimental studies of other researchers.
[b] Accelerated flow.
[c] Movement of arm during simulation.
[d] Steady approach flow but unsteady wake flow.

predictions of wall friction, and thus of the boundary-layer separation locations, in most complex three-dimensional flows with separation and of boundary-layer transition from a laminar to a turbulent boundary layer (Barber et al., 2009; Casey and Wintergerste, 2000). Instead, the boundary layer can be resolved explicitly with low-Reynolds number modelling (LRNM), which should yield more accurate results but requires a much higher grid resolution in the boundary-layer region.

Detailed validation experiments are therefore required to quantify the accuracy of the applied CFD modelling techniques for a specific flow problem. Most CFD validation studies in sports aerodynamics (see Table 1: Barber et al., 2009; Bixler et al., 2007; Dabnichki and Avital, 2006; Gardano and Dabnichki, 2006; Meile et al., 2006) looked at drag and lift forces but extensive comparison of flow quantities, i.e. velocities or surface pressures, was generally not performed, except qualitatively, i.e. by means of flow visualisation. Such flow-field data provide complementary information to the drag measurements: a good agreement with CFD for drag is not necessarily the result of a correct flow-field calculation since the drag force is actually an integrated flow quantity (of surface pressures). An attempt to provide more detailed flow-field evaluation data for sport applications was presented by Defraeye et al. (2010). They performed wind-tunnel measurements on a cyclist where, apart from drag, also surface pressures were measured on 30 locations on the cyclist's body. However, the use of a real cyclist limited the amount of sensors and introduced some uncertainty on the pressure data, which was related to the determination of the exact locations of the pressure plates on the cyclist's body, the size of these plates and the attachment of the plates onto the body. Improvements could be obtained by using a (scale) model of a cyclist.

In this study, wind-tunnel experiments on such a scale model of a cyclist are presented. Apart from three-component forces and moments, also high-resolution surface pressure measurements on the scale model's surface are performed, i.e. at 115 locations. These wind-tunnel data are used to compare the performance of several commonly available turbulence-modelling approaches and boundary-layer modelling approaches of CFD. A comparison with the measured surface pressures provides more insight in the accuracy and deficiencies of each CFD modelling approach, than an evaluation only based on (drag) forces. The conclusions of this study can also be relevant for CFD studies involving high-speed applications of similar bluff-body geometries, such as swimmers, skiers, bobsleighers, etc.

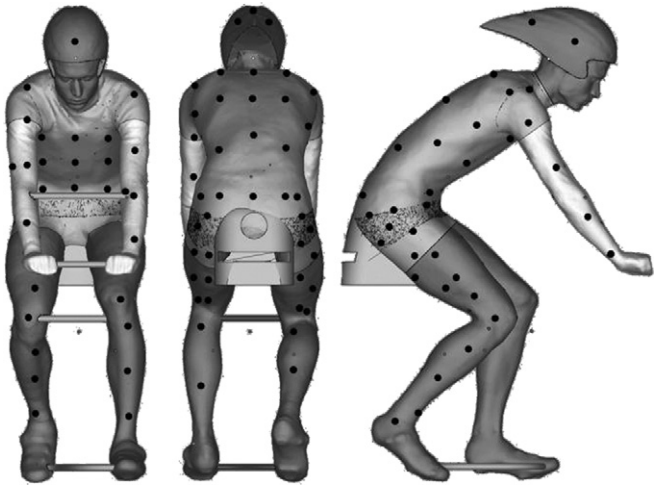

**Fig. 1.** Scale model of cyclist, manufactured by means of rapid prototyping. The locations of the pressure taps are shown schematically by means of black dots. The stiffening elements between the elbows and knees were not included in the actual scale model (see Fig. 2).

## 2. Methods

### 2.1. Experimental setup

A digital model of a cyclist in the upright position was obtained from a real cyclist (see Defraeye et al., 2010), using a high-resolution 3D laser scanning system (K-Scan, Nikon Metrology, Belgium) combined with post-processing software (Focus RE, Nikon Metrology, Belgium). This digital model was used as an input for the manufacturing process of the scale model (see Fig. 1) by means of rapid prototyping (scale 1:2). The bicycle was not included in the scale model for CFD meshing purposes and to reduce the manufacturing costs and the complexity of the scale model. Additional stiffening elements, with an aerodynamic shape, were included. The surface of the scale model was given a smooth finishing by resin impregnation. A total of 115 pressure taps were included in the scale model (see Fig. 1), placed flush with the surface, and were connected by pressure tubes (inside the hollow scale model) to the pressure transducer. The scale model was fixed on a stand (Fig. 2), where the upper part was given an airfoil-like profile to minimise drag. The half-sphere in Fig. 2, which is also a part of the stand, was required to house the pressure transducer since it had to be located close to the scale model to limit the length of the pressure tubes. The scale model and stand were placed in the test section (2.25 m high and 3 m wide) of a closed-circuit wind tunnel (German–Dutch Wind tunnels, Marknesse, The Netherlands) on a six-component force balance, located below the test-section floor.

Measurements were carried out at a wind speed of 20 m/s and the turbulence intensity at the inlet of the test section was 0.02%. The wind direction was parallel to

the (virtual) bicycle axis, representing head wind. The frontal areas of the scale model with stand and the stand separately are 0.23 and 0.11 $m^2$, respectively, resulting in a blockage ratio of 3% for the scale model with stand. All three force components ($F_x$, $F_y$ and $F_z$) and moment components ($M_x$, $M_y$ and $M_z$) were measured. The precision of the balance was 0.1% of the full-scale range, namely 0.25 N for $F_x$ (lateral) and $F_y$ (drag), 0.5 N for $F_z$ (lift), 0.09 N m for $M_x$ (pitch) and $M_y$ (roll) and 0.05 N m for $M_z$ (yaw). The balance data were sampled at 10 Hz for 30 s. Surface pressures on the scale model's surface were measured with pressure taps with an accuracy of 7 Pa, i.e. 0.1% of the full-scale range. The pressures were sampled at 512 Hz for 24 s.

Note that since a scale model has been used (scale 1:2 at a wind speed of 72 km/h, i.e. 20 m/s), the Reynolds number of these experiments is lower than for real cyclists at racing speeds (real scale at wind speeds of $\pm$50 km/h). Reynolds number effects during wind-tunnel tests at higher wind speeds (25–35 m/s) were however limited, namely about 2% for drag force, lift force and pitching moment, and on average 15% for surface pressures (see Section 3.1). Also note that the approach-flow conditions in the wind-tunnel tests in this study and in most other wind-tunnel experiments on cyclist aerodynamics (i.e. low turbulence intensity and a uniform velocity profile) are representative for the case where only the cyclist is moving and where the wind speed of the surrounding air is zero. This situation is typically found in indoor environments (e.g. a velodrome) or in the outdoor environment if there is no or little wind.

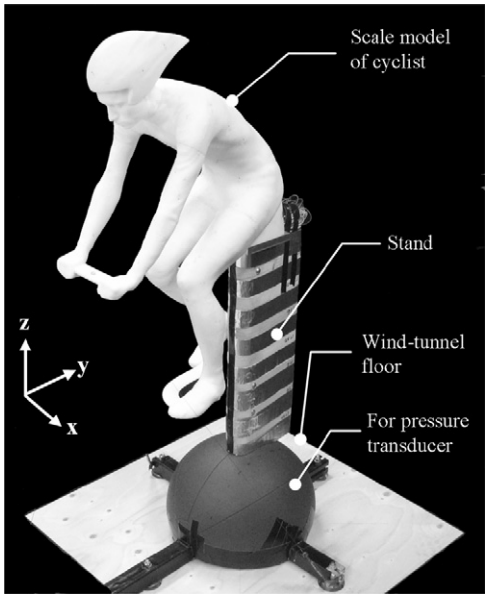


**Fig. 2.** Scale model with stand which is mounted on the wind-tunnel floor. The pressure transducer is located in the half-sphere.

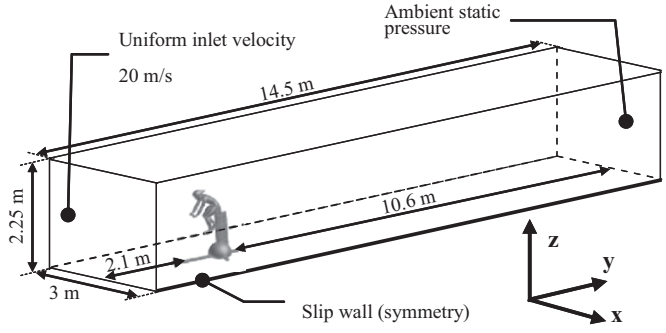


**Fig. 3.** Computational domain and boundary conditions.

### 2.2. Numerical simulations

#### 2.2.1. Numerical model

A digital model of the scale model together with stand (as in Fig. 2) was obtained using the 3D laser scanning system and was used for computational modelling. This virtual scale model was placed in a computational domain, representing the wind tunnel. The size of this domain and the imposed boundary conditions are specified in Fig. 3 (see Appendix A for additional information on the computational model).

#### 2.2.2. Simulation parameters

The simulations are performed with the CFD software Fluent 6.3, which uses the control volume method. Steady RANS is used in combination with different turbulence models: standard $k$–$\varepsilon$ model (Launder and Spalding, 1972), realizable $k$–$\varepsilon$ model (Shih et al., 1995), RNG $k$–$\varepsilon$ model (Choudhury, 1993), standard $k$–$\omega$ model (Fluent, 2006; Wilcox, 1988; Wilcox, 1998) and the shear-stress transport (SST) $k$–$\omega$ model (Menter, 1994). All these models are used with LRNM to take care of the viscosity-affected region, i.e. the boundary layer on the scale model's surface. Note that the $k$–$\varepsilon$ models require low-Reynolds number modifications since they were primarily developed for high-Reynolds number flows. Thereby, a two-layer approach is used where the turbulent core region of the flow is resolved with the $k$–$\varepsilon$ model and a low-Reynolds number model is used to resolve the viscosity-affected region, for which the one-equation Wolfshtein model (Wolfshtein, 1969) is used in this study. Note that this one-equation low-Reynolds number model is less complex than those used by the two-equation $k$–$\omega$ models since it only solves one transport equation for turbulence instead of two, which can lead to a reduced performance for some flow regimes. Of these turbulence models, the realizable $k$–$\varepsilon$ model is also used with wall functions since $k$–$\varepsilon$ models with wall functions are used in most aforementioned numerical studies in sports (see Table 1), and since they are included in most commercial CFD codes. Note that for the use of wall functions, the realizable $k$–$\varepsilon$ model is preferred over the standard $k$–$\varepsilon$ model for reasons of convergence stability. Two types of wall functions are used: standard (Launder and Spalding, 1974) and non-equilibrium (Kim and Choudhury, 1995) wall functions. Note that standard wall functions are only valid under equilibrium boundary-layer conditions (e.g. Casey and Wintergerste, 2000; Franke et al., 2007), which is not the case in regions of flow separation, reattachment and strong pressure gradients. For the LES simulations, the dynamic Smagorinsky subgrid-scale model is used (see Kim, 2004) with LRNM. An overview of the performed CFD simulations is given in Table 2 (see Appendix A for additional information on the simulations).

## 3. Results

### 3.1. Forces and moments

Aerodynamic forces are usually quantified by dimensionless coefficients, e.g. drag or lift coefficients. These force coefficients ($C_{Fx}$, $C_{Fy}$ and $C_{Fz}$) and moment coefficients ($C_{Mx}$, $C_{My}$ and $C_{Mz}$) relate the forces and moments to the frontal area $A$ ($m^2$) and the lever arm $L$ (m)

$$F_i = \frac{\rho U^2}{2} A C_{Fi} \quad (1)$$

$$M_i = \frac{\rho U^2}{2} A L C_{Mi} \quad (2)$$

**Table 2**
Overview of modelling specifications of the performed CFD simulations.

| Abbreviation | Turbulence-modelling approach | Turbulence model | Boundary-layer modelling approach |
|---|---|---|---|
| s$k$–$\varepsilon$ | Steady RANS | Standard $k$–$\varepsilon$ | LRNM (Wolfshtein model) |
| r$k$–$\varepsilon$ | Steady RANS | Realizable $k$–$\varepsilon$ | LRNM (Wolfshtein model) |
| rng$k$–$\varepsilon$ | Steady RANS | RNG $k$–$\varepsilon$ | LRNM (Wolfshtein model) |
| s$k$–$\omega$ | Steady RANS | Standard $k$–$\omega$ | LRNM |
| sst$k$–$\omega$ | Steady RANS | SST $k$–$\omega$ | LRNM |
| r$k$–$\varepsilon$_SWF | Steady RANS | Realizable $k$–$\varepsilon$ | Standard wall functions |
| r$k$–$\varepsilon$_NWF | Steady RANS | Realizable $k$–$\varepsilon$ | Non-equilibrium wall functions |
| LES | LES | Smargorinsky | LRNM |

where $\rho$ is the air density (kg/m$^3$), $U$ is the approach-flow wind speed (m/s) and $i$ is an index ($x$, $y$ or $z$). Often, the force or moment area ($AC_{Fi}$ and $ALC_{Mi}$) is reported, since this does not require an explicit determination of $A$ or $L$. Although $ALC_{Mi}$ actually has the dimensions m$^3$, it is referred to as moment area in this study. In Fig. 4, the dependency of the force and moment areas, from wind-tunnel experiments, with the approach-flow wind speed is indicated. These areas become quasi-independent of the Reynolds number at wind speeds $\geq 20$ m/s. The force and moment areas of the scale model with stand, obtained by the wind-tunnel experiments, are compared with the results from the various CFD simulations in Fig. 5, by reporting their relative difference. Note that $AC_{Fx}$, $ALC_{My}$ and $ALC_{Mz}$ are not compared since their value is very low due to symmetry, resulting in relatively large measurement errors. The measurement errors on $AC_{Fy}$ (drag area), $AC_{Fz}$ (lift area) and $ALC_{Mx}$ (pitch area) are 0.8%, 4.0% and 0.5%, respectively.

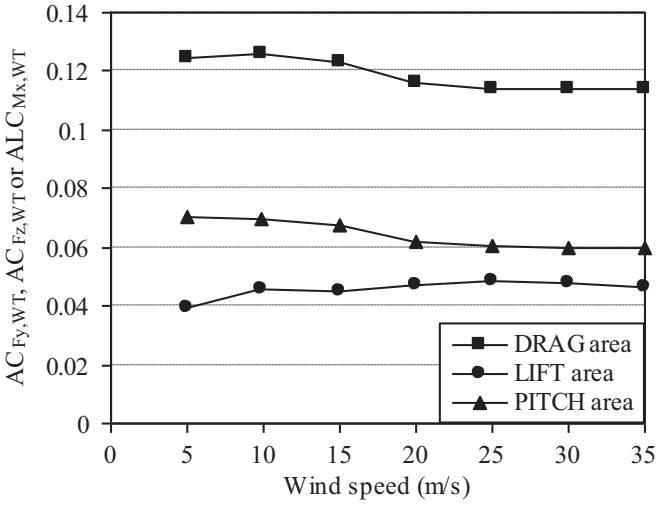


**Fig. 4.** Drag, lift and pitch areas (of scale model with stand) of wind-tunnel tests ($AC_{Fy,WT}$, $AC_{Fz,WT}$, $ALC_{Mx,WT}$) as a function of the approach-flow wind speed.

Some general trends can be distinguished in the CFD predictions: an underprediction of the drag and pitch areas by most turbulence models and an overprediction of the lift area. Apart from turbulence and boundary-layer model limitations, a possible reason for part of the differences with the wind-tunnel experiments could be a discrepancy in the boundary-layer thickness on the lower wall, which is a few centimetres in the wind tunnel. Since no exact information was available however, it was assumed in the CFD simulations that the thickness was zero at the inlet of the computational domain, resulting in a thickness of a few centimetres near the scale model. The influence of this boundary-layer mismatch is however considered quite limited. Since the stand itself also accounts for a significant part of the drag force, lift force and pitching moment, mainly due to its relatively large frontal area (50% of that of the scale model with stand), discrepancies with the wind-tunnel data are not only related to an erroneous prediction of flow around the scale model itself, but also around that of the stand, which is quantified and discussed in detail in Appendix A.

Of all LRNM $k$–$\varepsilon$ models, the standard model seems to show the best overall performance, where only the lift area is overpredicted significantly. The use of wall functions seems to decrease the accuracy to some extent, i.e. with about 7%, but no significant differences were found between the two wall-function types. For the $k$–$\omega$ models, the standard model shows large discrepancies with the wind-tunnel measurements, except for the lift area. The SST $k$–$\omega$ model however shows a very good agreement for both force and moment areas ($\leq 11\%$ with an

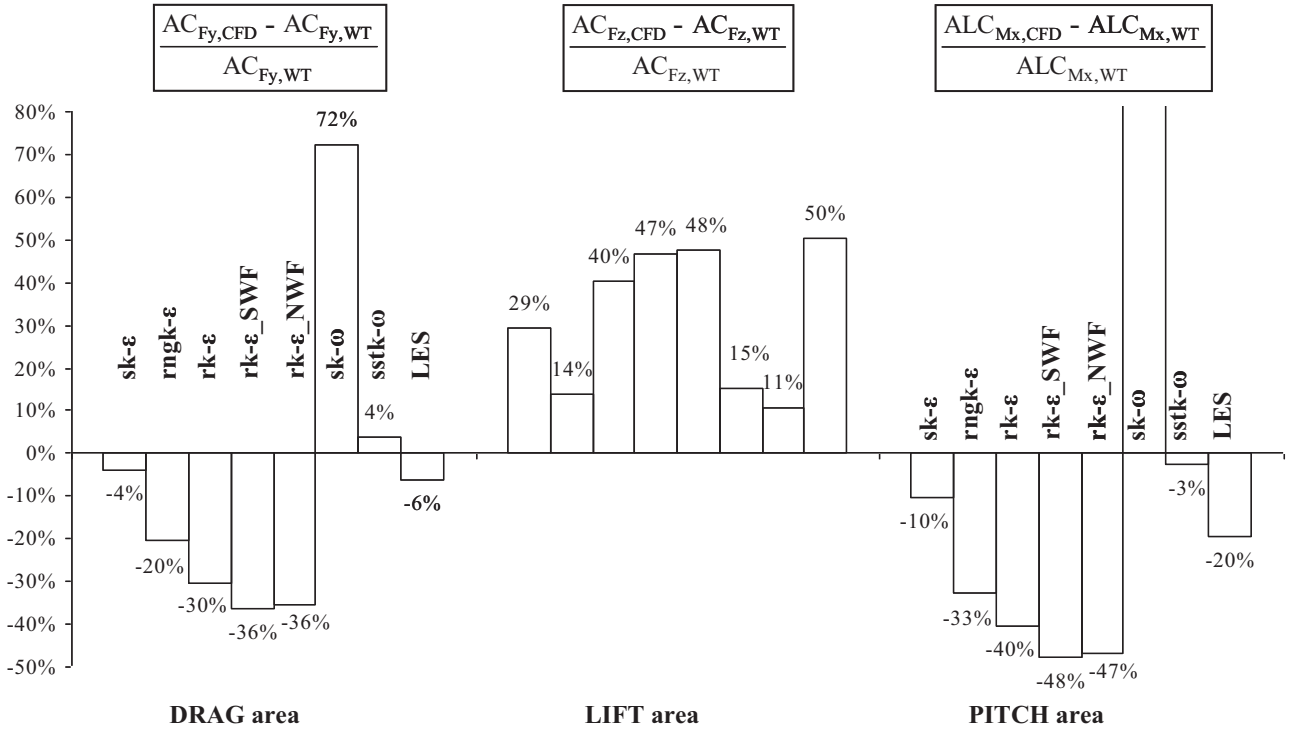


**Fig. 5.** Comparison of relative difference of drag, lift and pitch areas (of scale model with stand) of wind-tunnel tests ($AC_{Fy,WT}$, $AC_{Fz,WT}$, $ALC_{Mx,WT}$) and various CFD simulations ($AC_{Fy,CFD}$, $AC_{Fz,CFD}$, $ALC_{Mx,CFD}$). See Table 2 for the abbreviations of the CFD turbulence models.

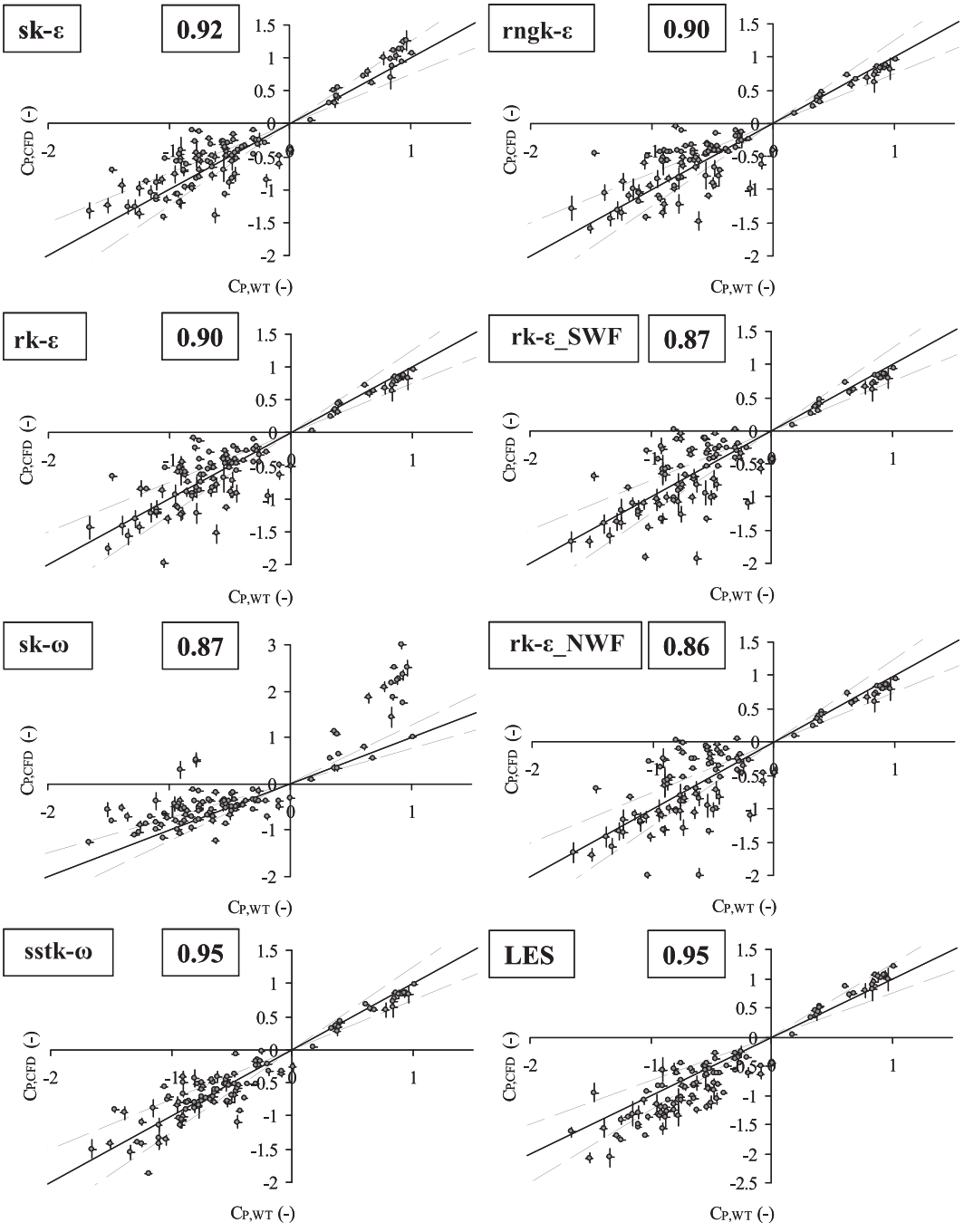


**Fig. 6.** Comparison between pressure coefficients of wind-tunnel tests ($C_{P,WT}$) and various CFD simulations ($C_{P,CFD}$) (with uncertainty bands). The correlation coefficients are also indicated. Note that the vertical axes of *sk–ω* and LES have a different scale. The uncertainty band for $C_{P,CFD}$ is the standard deviation from the averaged value within a circular zone (diameter 7 mm) on the surface of the scale model. For the uncertainty of $C_{P,WT}$, the measurement error on the pressure taps (7 Pa) is used. The dotted lines represent 25% deviation from the solid line. See Table 2 for the abbreviations of the CFD turbulence models.

average of 6%), and thereby it performs best of all evaluated turbulence-modelling approaches. Although LES provides relatively accurate drag and pitch area predictions, the lift area is severely overpredicted, which is mainly attributed to the stand (see Appendix A). Note however that an accurate prediction of force and/or moment areas does not necessarily imply that the flow field is resolved accurately, i.e. the prediction of over- and underpressure zones, since these areas are actually integrated quantities. Since flow-field information could provide additional insight for the comparison of CFD simulations, surfaces pressures on the scale model are evaluated in the next section.

### 3.2. Pressure coefficients

Surface pressures are usually expressed by dimensionless pressure coefficients ($C_P$)

$$C_P = \frac{(p_{surf} - p_{inl})}{\frac{\rho U^2}{2}} \tag{3}$$

where $p_{surf}$ is the pressure on the scale model's surface and $p_{inl}$ is the static pressure at the inlet of the wind-tunnel test section. For the CFD simulations, $p_{inl}$ is the average pressure at the inlet of the computational domain. Note however that this inlet is not located

at the same location as the inlet of the wind-tunnel test section, which is done to limit the size of the upstream part of the computational domain. In Fig. 6, the $C_P$ coefficients obtained with the wind-tunnel experiments ($C_{P,WT}$) are compared to the results from the CFD simulations ($C_{P,CFD}$) for different turbulence and boundary-layer modelling approaches. Due to the manufacturing process of the scale model and the generation of the digital model for the CFD simulations, which led to some smoothing out of surface details, there is some uncertainty on the locations of the pressure taps. To account for this uncertainty, the reported CFD data are the averaged pressures within a circular zone (diameter 7 mm) on the surface of the scale model. The uncertainty band for the CFD results in Fig. 6 is the standard deviation from this averaged value, and is quite small. For the uncertainty of the wind-tunnel data, the measurement error on the pressure taps (7 Pa) is used. Note that a good agreement of CFD with wind-tunnel measurements implies that the data are located near the solid line which is shown in the figures. The dotted lines represent 25% deviation from this solid line. A more straightforward comparison between the results of the different CFD simulations can be done by comparing the correlation coefficients (see Fig. 6). Additional information on the flow field is given in Appendix A.

Roughly the same trends are found as in the previous section: (1) of the LRNM $k$–$\varepsilon$ models, the standard $k$–$\varepsilon$ model shows the best performance; (2) the use of wall functions leads to a decreased accuracy, compared to LRNM; (3) of the $k$–$\omega$ models, the standard model does not perform well, especially for the windward pressures, while the SST $k$–$\omega$ model performs best of all evaluated turbulence-modelling approaches; (4) LES also performs very well, i.e. comparable with the SST $k$–$\omega$ model.

## 4. Discussion

The results of both the force and moment areas combined with the surface pressures allow a detailed comparison of the performance of the different turbulence and boundary-layer modelling approaches. Regarding turbulence modelling, RANS combined with the SST $k$–$\omega$ model clearly shows the best overall performance, but also LES performs very well, except for the lift area, which is mainly attributed to the stand (see Appendix A). Although LES outperforms all other RANS turbulence models and provides in addition information on the unsteady, i.e. temporally-fluctuating, flow field around the scale model, it however imposes a much higher computational cost (about 5–15 times more than RANS, depending on the RANS turbulence model used), which makes the RANS SST $k$–$\omega$ model more attractive from a practical point of view. The reason for the good performance of the SST $k$–$\omega$ model is probably because it uses a two-equation $k$–$\omega$ model formulation to solve the near-wall region, for which the $k$–$\omega$ models were originally developed, while a $k$–$\varepsilon$ model formulation, developed for high-Reynolds number flows, is used to solve the turbulent core region of the flow. If a $k$–$\omega$ model is used to resolve the turbulent core region, which is done in the standard $k$–$\omega$ model, clearly larger discrepancies with the experiments are found since this model was primarily not developed for resolving this region.

In this study, the standard $k$–$\omega$ model shows the worst performance of all LRNM RANS models which is in contrast to the study of Zaïdi et al. (2010), in which this model clearly outperformed the standard $k$–$\varepsilon$ model with respect to drag predictions. These findings could be related to the fact that a highly aerodynamic shape was considered by Zaïdi et al. (2010), namely a swimmer in diving position, combined with the use of a wall-function grid. For this flow problem, the wake zone is quite small and the skin-friction drag significantly contributes to the total drag: about 20%, compared to about 5% in this study. Thereby, the prediction of boundary-layer separation, which determines the size of the wake zone, and wall friction becomes critical for an accurate drag prediction, but the wall functions, used by the $k$–$\varepsilon$ models, generally cannot provide accurate predictions here (Casey and Wintergerste, 2000). The $k$–$\omega$ models, which are in essence developed to deal with near-wall, i.e. low-Reynolds number flows, could therefore provide more accurate results. The LRNM approach is clearly identified as a more accurate boundary-layer modelling alternative than wall functions in this study although LRNM requires a much higher grid resolution in the near-wall region, resulting in much more cells in the computational model, especially at high wind speeds (see Appendix A).

In many of the previous validation experiments (see Table 1) only drag and/or lift forces were quantified. Since these are integrated flow quantities, they do not necessarily imply accurate flow-field predictions. However, in this study, the detailed surface pressure measurements indicated that the accuracy of the different modelling approaches could be compared well by considering force and moment measurements. It is however important to note that a comparison based on only one parameter, e.g. the drag force, is not always sufficient. Therefore it is recommended to compare multiple parameters, as in Fig. 5, if possible together with flow-field evaluation.

## 5. Conclusions

In this study, a detailed experiment of flow around a scale model of a cyclist allowed an extensive comparison of various CFD modelling approaches. It was found that the RANS SST $k$–$\omega$ model showed the best overall performance, followed by the more computationally expensive LES, and that LRNM is clearly preferred over wall functions to model the boundary layer. This study showed that there are more accurate alternatives for evaluating flow around bluff bodies than the standard $k$–$\varepsilon$ model combined with wall functions, which is often used in CFD studies in sports. Although CFD did not provide the same accuracy as the wind-tunnel experiments in this study, it has the significant advantage that detailed flow-field information is available, which can contribute to the physical insight in the causes of the drag force. The results of this study can also be relevant for CFD studies involving high-speed applications of similar bluff-body geometries, such as swimmers, skiers, bobsleighers, etc. Note that for very aerodynamically-shaped bodies, e.g. a swimmer in diving position, the influence of the boundary-layer modelling approach will probably become even more critical.

## Conflict of interest statement

None.

## Acknowledgements

This study was funded by the Flemish Government and the Flemish Cycling Federation, which had no involvement in: study design, collection, analysis and interpretation of data; writing of the manuscript; the decision to submit the manuscript for publication. Special thanks go to Jos Smets (Belgian Cycling Federation), Eddy Willemsen and the DNW wind-tunnel team, Harry Sools and the SIRRIS team.

## Appendix A. Supplementary material

Supplementary data associated with this article can be found in the online version at doi:10.1016/j.jbiomech.2010.04.038.

## References


Barber, S., Chin, S.B., Carre, M.J., 2009. Sports ball aerodynamics: a numerical study of the erratic motion of soccer balls. Computers & Fluids 38 (6), 1091–1100.

Bixler, B., Pease, D., Fairhurst, F., 2007. The accuracy of computational fluid dynamics analysis of the passive drag of a male swimmer. Sports Biomechanics 6 (1), 81–98.

Bixler, B., Riewald, S., 2002. Analysis of a swimmer's hand and arm in steady flow conditions using computational fluid dynamics. Journal of Biomechanics 35 (5), 713–717.

Bixler, B., Schloder, M., 1996. Computational fluid dynamics. An analytical tool for the 21st century swimming scientist. Journal of Swimming Research 11, 4–22.

Casey, M., Wintergerste, T., 2000. Best Practice Guidelines. ERCOFTAC Special Interest Group on "Quality and Trust in Industrial CFD", ERCOFTAC.

Choudhury, D., 1993. Introduction to the renormalization group method and turbulence modeling. Fluent Inc. Technical Memorandum TM-107.

Dabnichki, P., Avital, E., 2006. Influence of the position of crew members on aerodynamics performance of a two-man bobsleigh. Journal of Biomechanics 39 (15), 2733–2742.

Defraeye, T., Blocken, B., Koninckx, E., Hespel, P., Carmeliet, J., 2010. Aerodynamic study of different cyclist positions: CFD analysis and full-scale wind-tunnel tests. Journal of Biomechanics 43 (7), 1262–1268.

Fluent, 2006. Fluent 6.3 User's Guide. Lebanon–New Hampshire, USA.

Franke, J., Hellsten, A., Schlünzen, H., Carissimo, B., 2007. Best practice guideline for the CFD simulation of flows in the urban environment. COST Action 732: Quality assurance and improvement of microscale meteorological models, Hamburg.

Gardano, P., Dabnichki, P., 2006. On hydrodynamics of drag and lift of the human arm. Journal of Biomechanics 39 (15), 2767–2773.

Grappe, G., Candau, R., Belli, A., Rouillon, J.D., 1997. Aerodynamic drag in field cycling with special reference to the Obree's position. Ergonomics 40 (12), 1299–1311.

Hanna, R.K., 2002. Can CFD make a performance difference in sport?. In: Ujihashi S., Haake, S.J. (Eds.), The Engineering of Sport 4. Blackwell Science, Oxford, pp. 17–30.

Kim, S.-E., 2004. Large eddy simulation using unstructured meshes and dynamic subgrid-scale turbulence models. In: Proceedings of the 34th AIAA Fluid Dynamics Conference and Exhibit, Technical Report AIAA-2004-2548. Portland, Oregon.

Kim, S.E., Choudhury, D., 1995. A near-wall treatment using wall functions sensitized to pressure gradient. In: ASME FED, Separated and Complex Flows, vol. 217, ASME.

Kyle, C.R., Burke, E.R., 1984. Improving the racing bicycle. Mechanical Engineering 106 (9), 34–45.

Launder, B.E., Spalding, D.B., 1972. Lectures in Mathematical Models of Turbulence. Academic Press, London, England.

Launder, B.E., Spalding, D.B., 1974. The numerical computation of turbulent flows. Computer Methods in Applied Mechanics and Engineering 3 (2), 269–289.

Lecrivain, G., Slaouti, A., Payton, C., Kennedy, I., 2008. Using reverse engineering and computational fluid dynamics to investigate a lower arm amputee swimmer's performance. Journal of Biomechanics 41 (13), 2855–2859.

Lukes, R.A., Hart, J.H., Chin, S.B., Haake, S.J., 2004. The aerodynamics of mountain bicycles: the role of computational fluid dynamics. In: Hubbard, M., Mehta, R.D., Pallis, J.M. (Eds.), The Engineering of Sport. International Sports Engineering Association, Sheffield, pp. 5.

Meile, W., Reisenberger, E., Mayer, M., Schmölzer, B., Müller, W., Brenn, G., 2006. Aerodynamics of ski jumping: experiments and CFD simulations. Experiments in Fluids 41, 949–964.

Menter, F.R., 1994. Two-equation eddy-viscosity turbulence models for engineering applications. AIAA Journal 32 (8), 1598–1605.

Minetti, A.E., Machtsiras, G., Masters, J.C., 2009. The optimum finger spacing in human swimming. Journal of Biomechanics 42, 2188–2190.

Rouboa, A., Silva, A., Leal, L., Rocha, J., Alves, F., 2006. The effect of swimmer's hand/forearm acceleration on propulsive forces generation using computational fluid dynamics. Journal of Biomechanics 39 (7), 1239–1248.

Shih, T.H., Liou, W.W., Shabbir, A., Yang, Z., Zhu, J., 1995. A new $k$–$\varepsilon$ eddy viscosity model for high Reynolds number turbulent flows. Computers & Fluids 24 (3), 227–238.

Wilcox, D.C., 1988. Reassessment of the scale-determining equation for advanced turbulence models. AIAA Journal 26 (11), 1299–1310.

Wilcox, D.C., 1998. Turbulence modeling for CFD. DCW Industries Inc., La Canada, California, USA.

Wolfshtein, M., 1969. The velocity and temperature distribution in one-dimensional flow with turbulence augmentation and pressure gradient. International Journal of Heat and Mass Transfer 12 (3), 301–318.

Zaïdi, H., Taiar, R., Fohanno, S., Polidori, G., 2008. Analysis of the effect of swimmer's head position on swimming performance using computational fluid dynamics. Journal of Biomechanics 41 (6), 1350–1358.

Zaïdi, H., Fohanno, S., Taiar, R., Polidori, G., 2010. Turbulence model choice for the calculation of drag forces when using the CFD method. Journal of Biomechanics 43 (3), 405–411.